TISSUE ENGINEERING: Part A
Volume 30, Numbers 11 and 12, 2024
© Mary Ann Liebert, Inc.
DOI: 10.1089/ten.tea.2023.0194

termis
Tissue Engineering
& Regenerative Medicine
International Society

Open camera or QR reader and scan code to access this article and other resources online.

Downloaded by UNIVERSITY OF SOUTHERN CALIFORNIA PACKAGE from www.liebertpub.com at 08/21/25. For personal use only.

SPECIAL ISSUE: BIOPRINTING

4D Printed Nerve Conduit with *In Situ* Neurogenic Guidance for Nerve Regeneration

Haitao Cui, PhD,[1,2,*] Wei Zhu, PhD,[2,*] Shida Miao, PhD,[2] Kausik Sarkar, PhD,[2] and Lijie Grace Zhang, PhD[2–5]

Nerve repair poses a significant challenge in the field of tissue regeneration. As a bioengineered therapeutic method, nerve conduits have been developed to address damaged nerve repair. However, despite their remarkable potential, it is still challenging to encompass complex physiologically microenvironmental cues (both biophysical and biochemical factors) to synergistically regulate stem cell differentiation within the implanted nerve conduits, especially in a facile manner. In this study, a neurogenic nerve conduit with self-actuated ability has been developed by *in situ* immobilization of neurogenic factors onto printed architectures with aligned microgrooves. One objective was to facilitate self-entubulation, ultimately enhancing nerve repairs. Our results demonstrated that the integration of topographical and *in situ* biological cues could accurately mimic native microenvironments, leading to a significant improvement in neural alignment and enhanced neural differentiation within the conduit. This innovative approach offers a revolutionary method for fabricating multifunctional nerve conduits, capable of modulating neural regeneration efficiently. It has the potential to accelerate the functional recovery of injured neural tissues, providing a promising avenue for advancing nerve repair therapies.

Keywords: 4D printing, *in situ* immobilization, self-morphing, microgroove, nerve repair

Impact Statement

The burgeoning field of 4D printing technology has opened new avenues for fabricating intelligent structures and devices capable of dynamic transformations over time. This study demonstrates the development of a novel neurogenic nerve conduit with self-actuated ability by combining photolithography-stereolithography-tandem printing and *in situ* immobilization of neurogenic factors to achieve self-entubulation for nerve repair. As a revolutionary method, our combinational strategy integrating topographical and *in situ* biological cues into the printed conduits could significantly improve neural alignment and enhance neural differentiation.

Introduction

Neurological diseases and injuries, such as Parkinson's and Alzheimer's disease, peripheral nerve injury, traumatic brain injury as well as spinal cord injury, represent some devastating clinical challenges worldwide.[1–3] However, the regenerative capacity of the nervous tissue is severely deficient, and the use of autologous grafts has its drawbacks, including donor site morbidity and poor functional recovery.[3,4] As a promising therapeutic strategy, stem

[1]Key Laboratory of Biorheological Science and Technology, Ministry of Education, College of Bioengineering, Chongqing University, Chongqing, China.
Departments of [2]Mechanical and Aerospace Engineering, [3]Electrical and Computer Engineering, [4]Biomedical Engineering, and [5]Medicine, The George Washington University, Washington, District of Columbia, USA.
*These authors contributed equally to this work.

Downloaded by UNIVERSITY OF SOUTHERN CALIFORNIA PACKAGE from www.liebertpub.com at 08/21/25. For personal use only.

cell-based neural engineering offers the potential to replenish nerve cells and neurotrophic factors, thereby stimulating axonal growth and repair to rebuild severed axons and restore locomotor function.[2,4–6]

Various fabrication technologies have been explored to create artificial nerve conduits or guides with aligned channel/groove guidance for nerve regeneration.[7–12] This aligned design plays an important role in inducing neurite elongation along a preferred proximal-distal direction of stumps.[9,10,13] Compared to conventional fabrication techniques, 3D printing technology stands out as it enables the fabrication of patient-specific nerve conduits or constructs with precise and uniform patterns in various shapes and dimensions to meet clinical needs.[3,14–17] Beyond it, a recent concept known as 4D printing has emerged, involving the 3D printing of objects capable of self-morphing in structure or function under predetermined stimuli.[18–22] This novel approach sheds light on advancing the development of stimuli-responsive scaffolds, dynamic tissue niches, biorobots, and other biomedical devices.[18–20]

Recently, 4D platforms have been established for applications in minimum invasive surgeries and controllable transformation of fabricated scaffold architectures.[23–26] For instance, taking advantage of the self-morphing capacity, cardiac patches fabricated using 4D printing have demonstrated improved dynamic integration with the beating heart[27] or enabled the creation of uniform tissues with adjustable curvatures.[28] In the context of stem cell regulation, programmable culture substrates manufactured through 4D printing have been utilized to improve the neurogenic differentiation of neural stem cells along with axial elongation in a spatiotemporal manner.[29] Moreover, we have developed a proof-of-concept 4D nerve conduit using a multi-responsive 4D plus printing technique, offering multifunctionality for neural tissue engineering.[23,30]

In addition, other researchers have successfully developed 4D printed nerve conduits for enhancing the repair of sciatic nerve defects in rat model.[31] Their results demonstrated that dynamic 4D transformation could achieve self-entubulation and seamless integration with injured nerves. While this innovative manufacturing strategy provides a facile method to generate self-morphing conduits for improved nerve tissue integration, there are certain limitations, especially regarding the choice of limited 4D materials and their biofunctionality. The physical guidance provided by microstructures has not been fully explored, and the lack of effective bioactivity has hindered significant improvement in nerve regeneration, especially concerning clinical demands. Addressing these challenges will be crucial for unlocking the full potential of 4D printed nerve conduits in nerve tissue engineering and regeneration.

In this study, nerve conduits containing various microgroove (or microchannel) densities were fabricated using a biobased material and photolithography-stereolithography-tandem (PST) printing, which are expected to achieve self-entubulation of grafts with injured nerves and guide axonal alignment within the conduits. To further enhance neural regeneration, multiple growth factors (GFs) were immobilized onto the printed conduits using the biocompatible, mussel-inspired adhesion chemistry. Compared to other carrier methods, this nontoxic mussel-inspired chemistry offers a highly efficient approach for immobilizing biologics, ensuring sustainable bioactivity of released factors, and potentially addressing the challenge of prolonged tissue retention.[32–34]

With the overarching goal of improving neural functions and neural differentiation behaviors, our study presents a novel method to create a conducive microenvironment inside a smart conduit with morphing ability (Fig. 1). This integrated microenvironment incorporates both topographic

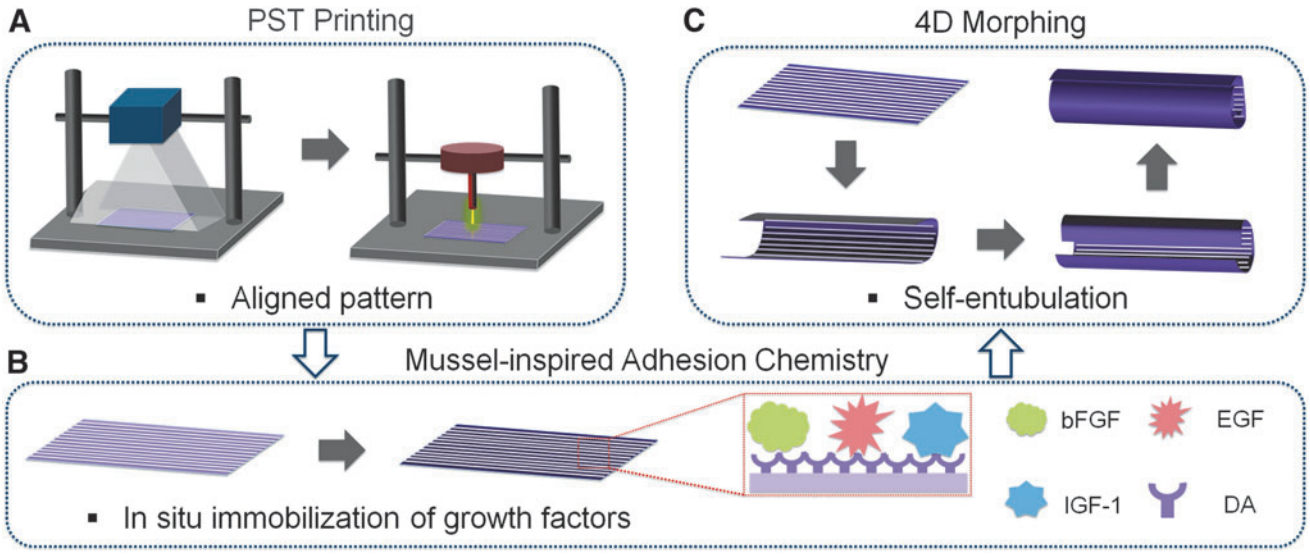

FIG. 1. Schematic illustration of the fabrication process of a 4D printed nerve conduit with *in situ* neurogenic guidance. **(A)** Nerve conduit scaffolds are fabricated using PST printing. **(B)** Neurogenic GFs, including DA, bFGF, EGF, and IGF-1, are *in situ* immobilization by mussel-inspired adhesion chemistry. **(C)** The nerve conduit scaffolds undergo a 4D morphing process. bFGF, basic fibroblast growth factor; DA, dopamine; EGF, epidermal growth factor; GF, growth factor; IGF-1, insulin-like growth factor 1; PST, photolithography-stereolithography-tandem.

and biological factors, working synergistically to enhance *in situ* neurogenic differentiation and support aligned axonal growth, ultimately promoting nerve regeneration.

Materials and Methods

Ethics statement

All experiment methods were performed in accordance with relevant guidelines and regulations. There are no animal and human subjects involved in this study, so IRB approval is not applicable.

Preparation of 3D printable ink

Soybean oil epoxidized acrylate (SOEA; Sigma) and Irgacure 819 (bis(2,4,6-trimethylbenzoyl)-phenylphosphineoxide, Ciba) (1/80 w/w) were homogeneously mixed in acetone to obtain a yellow solution. The mixture was then vacuumed in the dark overnight to obtain a sticky ink for printing.

Scaffold (conduit) design and PST printing

PST printing refers to a combinational printing strategy of photolithography (PL) and stereolithography (SL) used in tandem.[25] The predesigned macrostructure of scaffolds was printed by PL with a photomask, and then a thin ink layer ($\sim 10\,\mu m$) was left after PL, which is a crucial feature for the next step of topographic formation. After that, the uncured thin layer was subsequently printed via our customized beam-scanning SL system. The SL system includes a 200 μm laser fiber with 355 nm UV light (max. 15 kHz and 20 μJ; MarketTech). Topographic patterns were designed with Autodesk123D software (Autodesk Inc.). Then the generated .stl file was uploaded into the Slic3r. The infill density was set to obtain different microgroove densities of scaffolds. Finally, the scaffolds were printed and then put in ethanol to remove uncured material. Before use, the conduits were sterilized with 75% ethanol and rinsed with phosphate-buffered saline (PBS) solution.

Characterization

Shape morphing was recorded in a UV transilluminator system (Ultra Lum). The ink containing 0.01% Fluorescein (Alfa Aesar) or Nile red (Sigma) was used to print the yellow- or red-colored samples. After 4D shape changing, the images were taken with a camera (Cannon; PowerShot ELPH 360HS). After coating with a ~ 10 nm gold layer, the surficial morphology of conduits (partial area) was observed with a scanning electron microscope (SEM) with a 5 kV electron beam (Zeiss SigmaVP). The surficial images of conduits were visualized with microscopy (Mu800; Amscope), where the surface plots plug-in was used to analyze the surface topography.

Cell culture

Human mesenchymal stem cells (hMSCs with passage No. 3–6, from bone marrow; the Texas A&M Health Science Center) were cultured in an MSC growth medium. The MSC growth medium was prepared by mixing alpha minimum essential medium (α-MEM plus L-glutamine), 20% fetal bovine serum (FBS), and 1% (v/v) penicillin/streptomycin.

Cell alignment analysis

To optimize the infill densities, hMSCs (1×10^5 cells/cm^2) were cultured on the micropatterned scaffolds for 3 days. After fixing with formalin for 15 min, the cell-laden samples were soaked in Triton X-100 solution (0.1%) for 10 min of cell permeabilization. Then the samples were incubated with phalloidin (Texas red) solution for 20 min and 4′,6-diamidino-2-phenylindole (DAPI) solution for 3 min, respectively. Finally, a confocal microscope (Zeiss LSM 710) was used to image the samples (a local area of conduits), and NIH ImageJ software was used to quantitively analyze the hMSC alignment.[28,29] Here, the cell orientation was the direction of the major axis of cells to the microgroove (0°).

Surface modification and in situ *protein immobilization*

After the optimization, the dopamine (DA) chemistry was performed to immobilize the GFs on the patterned conduits for inducing the hMSC differentiation. In brief, a 2 mg/mL DA-Tris solution was prepared. The printed scaffolds were shaken in the DA solution at room temperature for 12 h in the presence of oxygen. After washing with distilled water, the polydopamine (pDA)-coated conduits were soaked in the protein solution for 24 h. Finally, to remove the unattached protein, the conduits were rinsed with PBS.

In addition, to investigate the protein immobilization capacity of the 4D conduits, bovine serum albumin (BSA) was used as a protein model. The conduits were incubated at 37°C in BSA solution (40 μg/mL) for 1 day, and the BCA™ protein assay (Thermo) was used to measure the concentration of protein immobilization. Moreover, the protein immobilization efficiency of pDA-coated scaffolds with different concentrations of proteins was also studied by immersing the scaffolds into different concentrations of BSA solution. According to the manufacturer's instructions, the absorbance at the wavelength of 562 nm was recorded using a microplate spectrophotometer (Multiskan GO, Thermo). The surface hydrophilicity of the different samples was also evaluated by a contact angle analyzer (DSA4, Kruss).

Cell proliferation study

hMSCs (3×10^4 cells/cm$_2$) were cultured on the conduits for 3, 5, and 7 days. After each time point, the Cell Counting Kit-8 (Dojindo) was used to analyze cell viability. The samples were incubated for 2 h, and the absorbance at the wavelength of 450 nm was measured using the microplate spectrophotometer. The cell morphology of the coated (and uncoated) micropatterned scaffolds was also evaluated after 7 days of culture by the double-staining of Texas red phalloidin and DAPI as we mentioned above, and the coated (and uncoated) flat samples were served as controls.

Neurogenic differentiation and immunofluorescence

The *in situ* GF immobilization samples were prepared with 0, 20, 50, and 100 ng/mL GF solutions. The solutions were prepared by mixing with an equivalent amount of insulin-like growth factor 1 (IGF-1), epidermal growth factor (EGF), and basic fibroblast growth factor (bFGF).[35–39] hMSCs (5×10^4 cells/cm^2) were cultured on the samples in the hMSC growth medium. After 2 weeks, the

Downloaded by UNIVERSITY OF SOUTHERN CALIFORNIA PACKAGE from www.liebertpub.com at 08/21/25. For personal use only.

Downloaded by UNIVERSITY OF SOUTHERN CALIFORNIA PACKAGE from www.liebertpub.com at 08/21/25. For personal use only.

conduits were collected to evaluate the hMSC differentiation into human neural stem cell like cells (hNSCs). For the neural differentiation, the cells were continuously cultured in the hMSC growth medium supplemented with 1 μM retinoic acid (RA). After another 2 weeks, the samples were collected to evaluate the neuronal and glial differentiation. After fixing with formalin and permeabilizing in Triton X-100 solution, the cells were blocked in a 1% BSA solution for 2 h.

After that, the cells were soaked in the primary antibody solution at 4°C overnight and then incubated in the second antibody solution for 2 h in the dark. The first primary antibodies (Abcam) were rabbit antimicrotubule-associated protein 2 (MAP2) antibody (1:500), rabbit anti-glial fibrillary acidic protein (GFAP) antibody (1:500), mouse anti-class-III β-tubulin (TuJ1) (1:1000), and rabbit anti-Nestin antibody (1:500). The secondary antibodies were goat anti-rabbit Alexa Fluor 488 (1:1000) and goat anti-mouse Alexa Fluor 594 (1:1000) (Thermo). Finally, the DAPI (1:1000) solution was used to stain the nuclei for 5 min. Fluorescence images of cells on a local area of conduits were taken using the confocal microscope.

Neurogenic gene expression

The gene expression of all conduits was analyzed by real-time quantitative polymerase chain reaction (rt-qPCR), including neurogenic differentiation 1 (ND1), neuron-specific enolase (NSE), Tau proteins (TAU), and neurogenin 2 (Ngn2) after 4 weeks of differentiation induction. A TRIzol reagent (Life Technologies) was used to extract the total RNA, and then a Prime ScriptRT Reagent Kit (TaKaRa) was used to reverse-transcribe to cDNA. Finally, a SYBR Premix Ex Taq (TaKaRa) reagent kit was used to conduct rt-qPCR via a CFX384 Real-Time System (BIO-RAD). The relative gene expression was calculated via the $2^{-\Delta\Delta}$Ct method, which was normalized against the control group. The housekeeping gene was beta-actin (β-actin). Primer sequences are shown in Table 1.

Statistical analysis

All experiments were conducted at least thrice, and $n \geq 9$ samples were tested. Data are shown as the mean ± standard deviation. A one-way analysis of variance (ANOVA) ($^*p < 0.05$; $^{**}p < 0.01$; $^{***}p < 0.001$) was performed with a *post hoc* Tukey's test to validate significant differences in data.

Experiment Results

Printing of nerve scaffolds

The SOEA ink was initially printed into predesigned structures using PL printing. Figure 2A shows the chemical reaction of SOEA during the printing process. In general, the scaffolds (with a thickness of ≤300 μm) exhibited autonomous rolling into complex structures after printing, allowing for the relaxation of internal stress. The different printed architectures resulted in various 4D shape changes in both orientation and angle (Fig. 2B). Moreover, an increase in printing speed led to a significant decrease in the thickness of printing objects, with a corresponding increase in their curvature (Fig. 2C).

Among the various structural designs, the rectangle macrostructure demonstrated the ability to achieve 4D rolling of the printed scaffolds, forming a tight scrolled conduit after the release of internal stress. This unique property makes it suitable for entubulating two stumps of the damaged or severed nerve. Therefore, it was selected to fabricate the conduit graft with morphing ability for the subsequent studies.

Microgroove pattern fabrication and cell alignment

Similar to our previous study,[25] the surficial micropatterns were fabricated on the printed conduits (scaffolds) using a unique PST printing technique. Unlike direct SL printing, PST printing enabled the generation of uniform and smooth micropattern structures on the surface of precured scaffolds. SEM images clearly displayed the formation of groove regions in non-SL areas, while ridge regions were generated in laser-illuminated areas (Fig. 3A). By varying the infill density of printing (40%, 60%, 80%, and 90%), a series of microgrooves were readily obtained with different widths, each with a depth of ~10 μm. The micropattern structure on the scaffolds was further analyzed using an optical microscope to generate corresponding 3D surface plot images (Fig. 3B).

To optimize cell alignment, hMSCs were seeded onto micropatterned scaffolds with different infill densities. Figure 3C illustrates the morphology of hMSCs on the scaffolds, identified by F-actin staining. The results revealed that hMSCs maintained a typical polygonal morphology on the surface of conduits. As the infill density increased, hMSC growth exhibited a more significant orientation. Moreover, quantification of hMSC alignment based on F-actin analysis (Fig. 3D) confirmed that the micropatterns effectively directed hMSC alignment. Scaffolds with higher infill density of microgrooves exhibited more ridges with narrower widths. Among the printed scaffolds, the fabricated micropatterns with ≥80% infill density displayed the highest efficiency of cell alignment.

Mussel-inspired chemistry and protein immobilization

BSA was tested to demonstrate the immobilization efficiency of GFs on the pDA-coated scaffolds, and the

Table 1. Primers of Quantitative Real-Time Polymerase Chain Reaction

Gene name	*Forward primer*	*Reverse primer*
β-actin	CCCTTGCCATCCTAAAAGCC	TGCTATCACCTCCCCTGTGT
ND1	CCACGGATCAATCTTCTCAG	CATGATGTGAATGGCTATCG
NSE	TAACTTCCGTAATCCCAGTGT	AAGAGGTCAGGTAAGCCAA
TAU	TACAGACCTGCGGCTTCATAA	CCAGAAATAGTCCTGCTCAACA
Ngn2	CCTGGAAACCATCTCACTTCA	TACCCAAAGCCAAGAAATGC

ND1, neurogenic differentiation 1; NSE, neuron-specific enolase; TAU, Tau proteins; Ngn2, neurogenin 2.

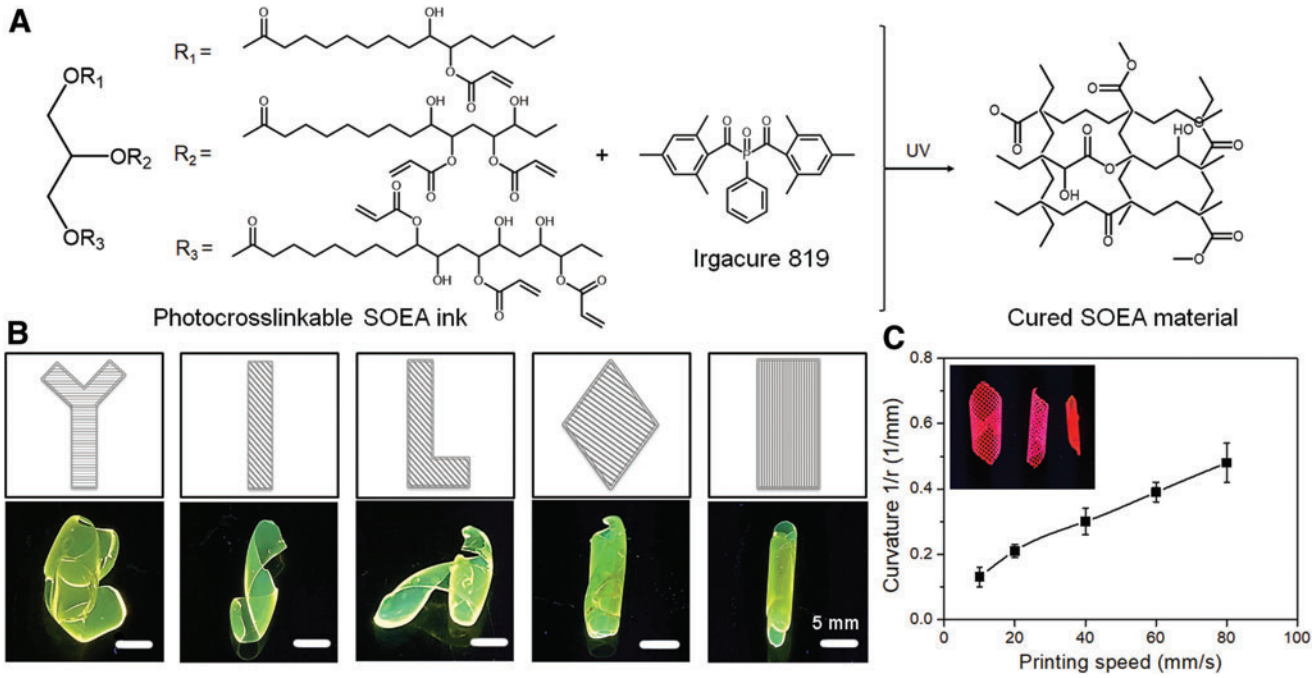

FIG. 2. 4D printing of nerve scaffolds (conduits). **(A)** Chemical reaction of SOEA during the printing process. **(B)** 4D morphing of various architectures with different printing paths, which were stained with Fluorescein dye. **(C)** Profile of curvature versus printing speed after 4D morphing of the printed structures, where the *inset* image shows the corresponding changing trend of Nile red-colored structures. SOEA, soybean oil epoxidized acrylate.

nontreated scaffolds served as the control. The adsorption profile showed that BSA levels on pDA-coated scaffolds were seven times higher than those on nontreated control after 24 h of immobilization (Fig. 4A). The protein immobilization study of pDA-coated scaffolds with different concentrations of proteins further demonstrated the highly efficient immobilization ability of GFs (Fig. 4B). In addition, a significant increase in hydrophilicity was observed on pDA-coated scaffolds compared to the SOEA controls. At the same time, there were minimal changes in wettability after protein immobilization (Fig. 4C). Moreover, hMSC proliferation was investigated to compare the difference between pDA-coated scaffolds and nontreated controls (Fig. 4D). After 7 days of culture, compared to the control group, the results showed improved hMSC proliferation over time.

hMSC growth and differentiation

To investigate the effect of pDA-coating and microgrooves on the growth and differentiation of hMSCs, hMSCs were incubated on various conduits for 1 and 2 weeks, including pDA-coated scaffolds with aligned patterns, nontreated scaffolds with aligned patterns, pDA-coated scaffolds without aligned patterns, and nontreated scaffolds without aligned patterns. The images showed that hMSCs formed a closely connected and continuous cellular sheet on the scaffolds. Notably, hMSCs on the aligned scaffolds exhibited excellent orientational growth along the microgrooves (Fig. 5A). The distribution of hMSC orientation on day 14 was further quantified based on the analysis of F-actin expression (Fig. 5B). The results demonstrated that hMSC alignment was more pronounced on the micropatterned scaffolds compared to the controls.

Next, the capability of hMSCs differentiating into human neural cells was evaluated to verify the efficacy of the printed aligned scaffolds with *in situ* immobilization of GFs in inducing neurogenesis. By varying the concentration of GFs from 0 to 100 ng/mL, the immunostaining of Nestin (a protein marker for neural stem cells, green) showed that concentration ≥50 ng/mL significantly promoted the neurogenic differentiation of hMSCs (Fig. 6). Moreover, cell alignment was significant on the printed aligned scaffolds, which is consistent with the hMSCproliferation results discussed above.

After an additional 2-week culture with RA supplement, the neuronal differentiation of hMSCs on various scaffolds was further evaluated using immunostaining and rt-qPCR analysis. Immunofluorescence analysis revealed significant neurogenesis on the scaffolds with GF immobilization regardless of their topologic patterns. The differentiated hMSCs on the printed scaffolds with *in situ* GF immobilization displayed prominent alignment of axons, identified by the neuron-specific marker TuJ1 (red) staining (Fig. 7). The GFAP expression (astrocyte marker, green) demonstrated significant astroglia genesis of hMSCs on the scaffolds with microgrooves and *in situ* GF immobilization. Furthermore, the positive expression of the mature neuronal marker MAP2 (green) confirmed the neurogenic maturation of hMSCs. Notably, compared to the samples without microgrooves, the expression levels of these neuronal markers on aligned scaffolds were elevated.

We conducted rt-qPCR analysis to quantitatively assess the neural differentiation of hMSCs after 4 weeks of differentiation culture. As shown in Figure 8, all neurogenic genes were significantly upregulated on the samples with

Downloaded by UNIVERSITY OF SOUTHERN CALIFORNIA PACKAGE from www.liebertpub.com at 08/21/25. For personal use only.

Downloaded by UNIVERSITY OF SOUTHERN CALIFORNIA PACKAGE from www.liebertpub.com at 08/21/25. For personal use only.

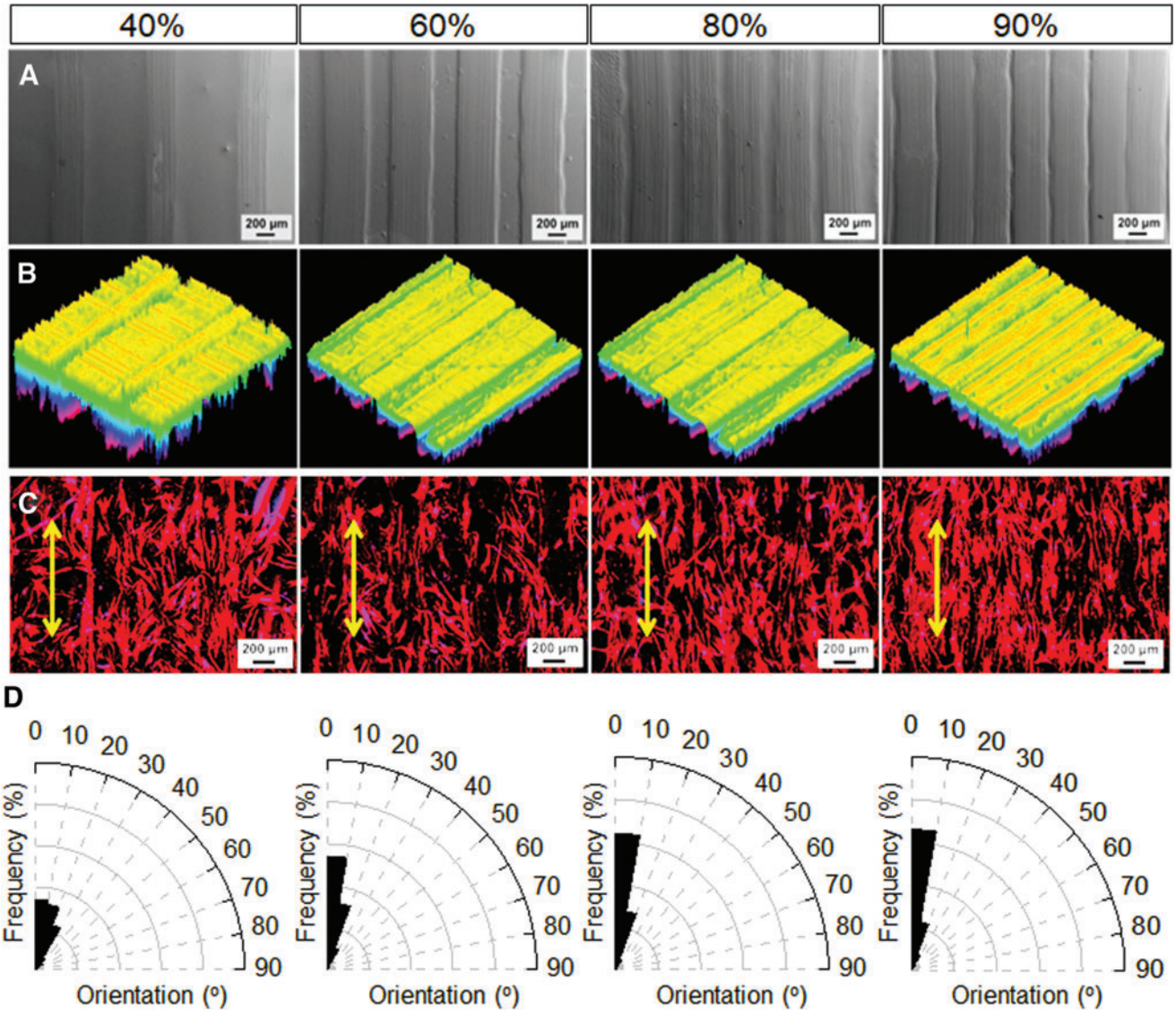

FIG. 3. Microgroove pattern fabrication and cell alignment. **(A)** SEM images of scaffolds with different widths (fill densities) of microgrooves. **(B)** 3D surface plot images of scaffolds with varying widths of microgrooves. **(C)** hMSC morphology on the scaffolds with microgrooves identified by F-actin staining, in which *yellow lines* with *double arrows* indicate the orientation of microgrooves. **(D)** Orientation analysis of hMSCs on the microgrooves with different widths. hMSCs, human mesenchymal stem cells; SEM, scanning electron microscope.

in situ immobilization compared to those without GFs. However, the expression of differentiating hMSCs on the aligned samples did not show significant enhancement for all genes.

Discussion

Biobased chemicals have garnered increased attention in recent years due to their excellent renewability, processability as well as biocompatibility. In recent studies, the biobased SOEA resin was used to fabricate tissue scaffolds using the SL printing technique.[25,40] Previous results from cell studies have also shown that SOEA offers advantages in photocuring ability and biocompatibility, similar to other biopolymers such as polyethylene glycol diacrylate, polycaprolactone (PCL), and polylactide.[23,25] The contact angle of the SOEA scaffolds is similar to PCL scaffolds, which might favor cell attachment.[25,40]

Moreover, our previous study has proposed a printing-induced 4D morphing mechanism based on the ''stress-relaxation'' phenomenon.[23,27] A light gradient intensity was generated in frontal polymerization as the light was attenuated in the ink solution.[23,27] This gradient in light attenuation within the resin induces the creation of a crosslink density gradient, resulting in the generation of internal stress that drives shape changes such as bending or folding.[23,27] The insufficient crosslinking reaction is responsible for the significant stress gradient observed. The different printed architectures also led to varied 4D shape changes in both orientation and angle, which can be attributed to the anisotropic stress relaxation of the patterned structures. It is expected that the simple approach would allow us to tailor

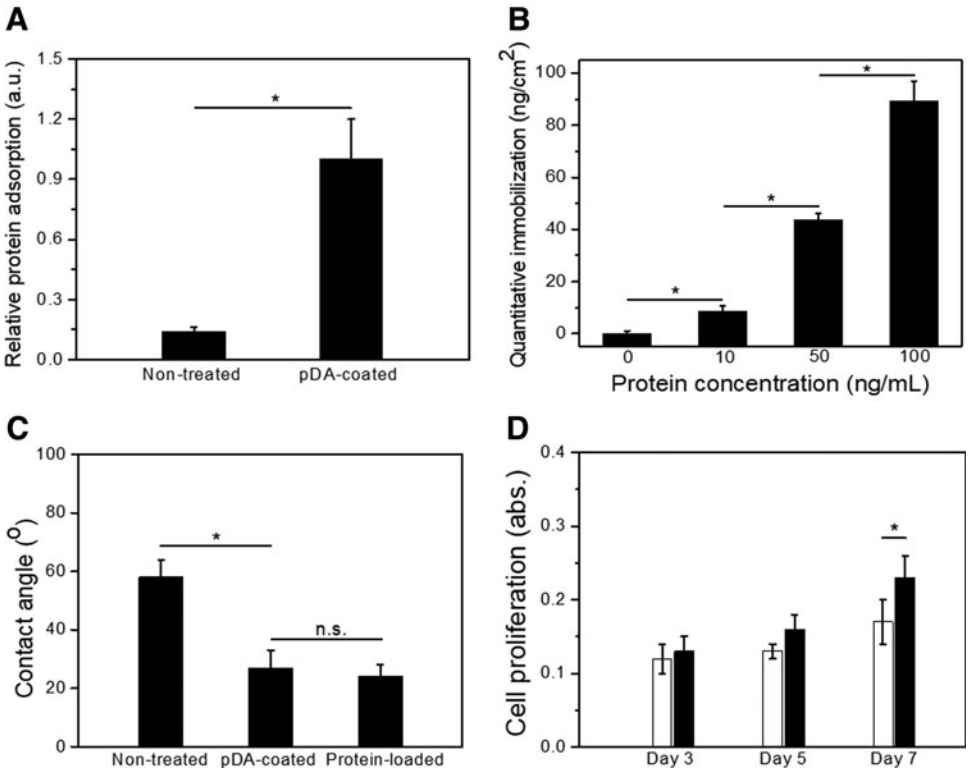

FIG. 4. Mussel-inspired chemistry and protein immobilization. **(A)** Relative protein absorption of pDA-coated scaffolds compared to the nontreated control. **(B)** Protein immobilization efficiency of pDA-coated scaffolds with varying concentrations of proteins. **(C)** Static contact angle measurements of nontreated, pDA-coated, and protein-loaded scaffolds. **(D)** hMSC proliferation on nontreated (*white bars*) and pDA-coated (*black bars*) scaffolds over a 7-day period. pDA, polydopamine.

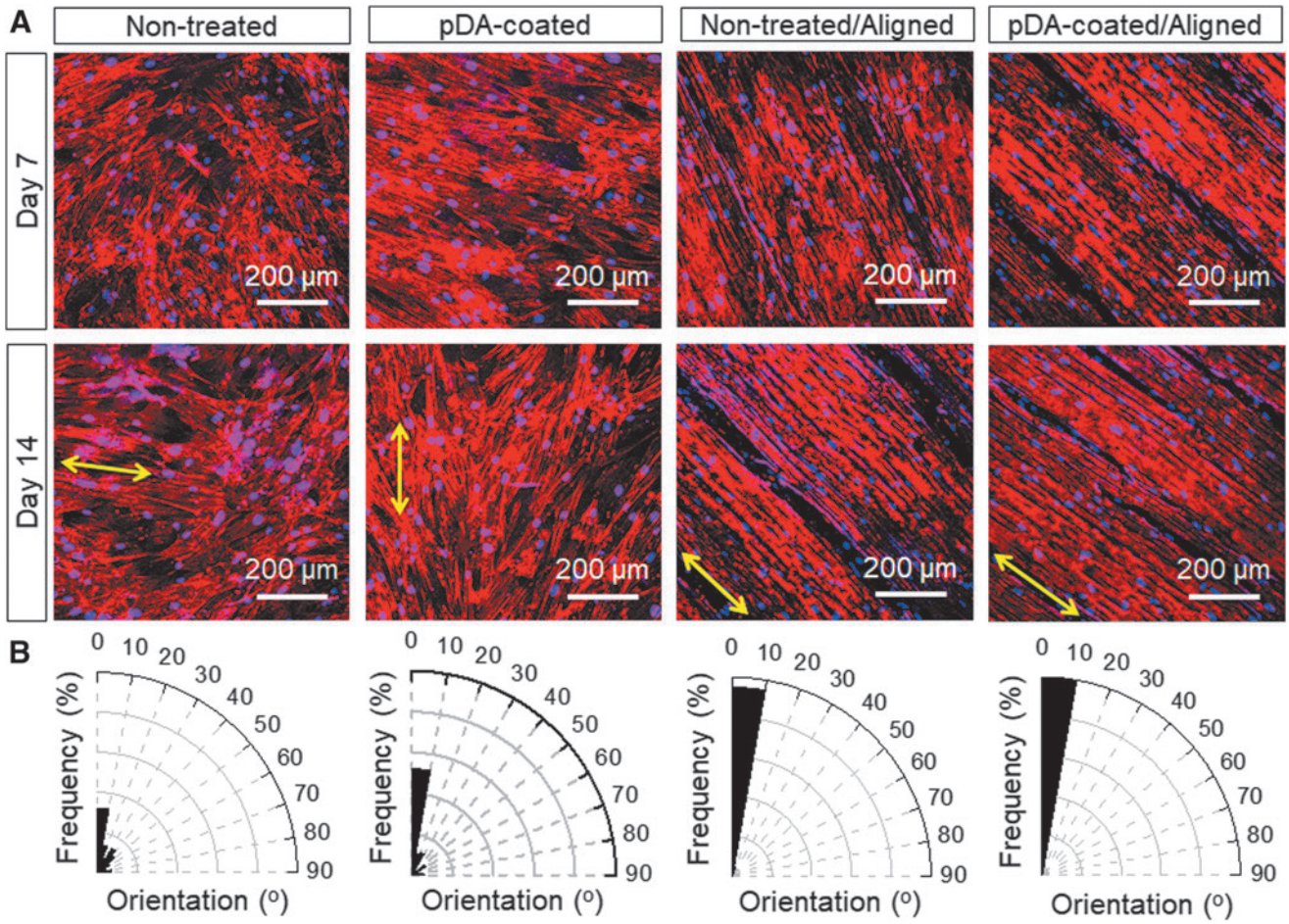

FIG. 5. hMSC growth on different scaffolds. **(A)** hMSC morphology on different scaffolds after 7 and 14 days of culture, identified by F-actin staining (DAPI, *blue*; F-actin, *red*). For nonaligned samples, *yellow lines* with *double arrows* show the major orientation of cell distribution, while for aligned samples, they indicate the orientation of microgrooves. **(B)** Orientation analysis of hMSCs on the scaffolds for day 14. DAPI, 4′,6-diamidino-2-phenylindole; hMSCs, human mesenchymal stem cells.

Downloaded by UNIVERSITY OF SOUTHERN CALIFORNIA PACKAGE from www.liebertpub.com at 08/21/25. For personal use only.

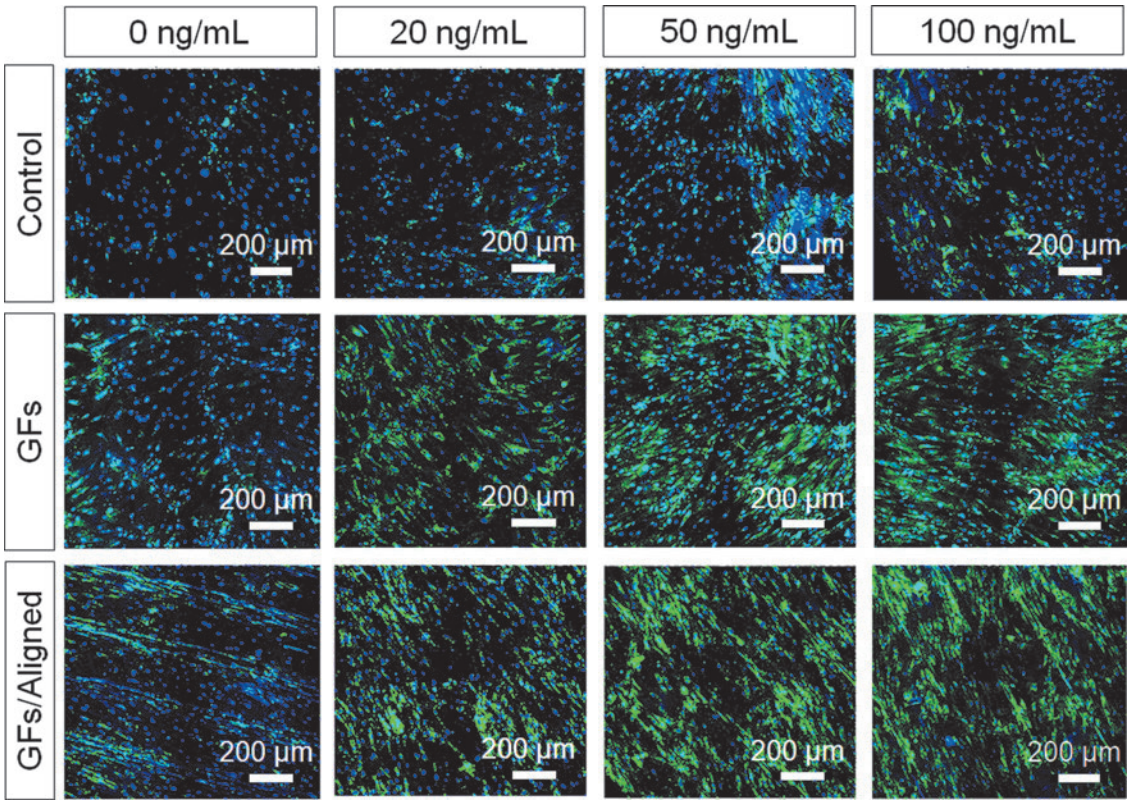

FIG. 6. Nestin staining of hMSC differentiation into hNSCs under different concentration conditions of immobilized GFs for 2 weeks (DAPI, *blue*; Nestin, *green*). Control, the nontreated scaffolds without aligned patterns; GFs, pDA/GFs-coated scaffolds without aligned patterns; and GFs/Aligned, pDA/GFs-coated scaffolds with aligned patterns. hMSC, human mesenchymal stem cell; hNSC, human neural stem cell like cell; pDA, polydopamine; DAPI, 4′,6-diamidino-2-phenylindole; GF, growth factor.

the printed objects to accommodate the varying curvatures of damaged tissues for achieving better tissue integration.

Similar to the 4D mechanism used in SL printing, PST printing was utilized for the sequential curing of photocrosslinkable ink alongside PL and SL printing. This process involved the initial creation of construct geometry through PL printing, followed by the application of SL printing to further cure a residually unsolidified layer on the scaffolds, thereby generating micropatterns on the inner surface. In comparison to using SL printing alone, this combined printing strategy revealed that the scaffolds not only possessed morphing ability but also exhibited intricate surface topography. In our study, we proposed the utilization of PST printing to construct a rectangular macrostructure, facilitating the fabrication of a self-actuated, tightly scrolled conduit with microgrooves (Fig. 2B).

This 4D rolling capability is anticipated to significantly enhance the seamless integration of damaged or severed nerves, while the highly aligned topographical cues may better guide topography-dependent axon alignment for neural regeneration. Moreover, the results of the hMSC adhesion and growth experiment confirmed that the highly aligned microgrooves resulted in efficient cell alignment.

Exogenous GFs have been used in previous studies to induce the neurogenic differentiation of hMSCs.[37,38,41,42] Since they are directly added to the culture medium, the targeted transport and sustained release of GFs are challenging to realize time- and dose-dependent kinetics in clinical research.[34] The immobilization of GFs potentially addresses these issues, providing sustainable bioactivity, site-specific delivery, and prolonged tissue retention.[43] Among various bioimmobilization techniques, nontoxic mussel-inspired chemistry has shown an efficient method for preparing multicomponent bioconjugated implants. In our study, through Michael's addition reaction, bFGF, EGF, and IGF-1 were immobilized onto printed neural conduits to promote the neurogenesis of hMSCs. The high binding affinity of Catechol groups to amines, thiol, and other nucleophiles facilitated its anchoring to proteins.[34,44]

The results of contact angle and cell proliferation experiments indicated that increased hydrophilicity and the deposition of nutritional components, such as FBS, even without GF immobilization, favored cell adhesion and proliferation. These findings also demonstrated the successful coating of pDA and adequate immobilization of multiple GFs on printed conduits.

As a multipotent cell population, hMSCs hold promise for various neurodegenerative diseases and injuries.[2,5,6] They are harvested from bone marrow, fat, blood, and other clinically accessible sources. hMSCs can self-renew and further differentiate into neural cell lines suitable for autologous transplantation.[4,5] Extensive studies have investigated the protocols for hMSC differentiation into human neural cells as well as the neurogenic function of GFs during

Downloaded by UNIVERSITY OF SOUTHERN CALIFORNIA PACKAGE from www.liebertpub.com at 08/21/25. For personal use only.

Downloaded by UNIVERSITY OF SOUTHERN CALIFORNIA PACKAGE from www.liebertpub.com at 08/21/25. For personal use only.

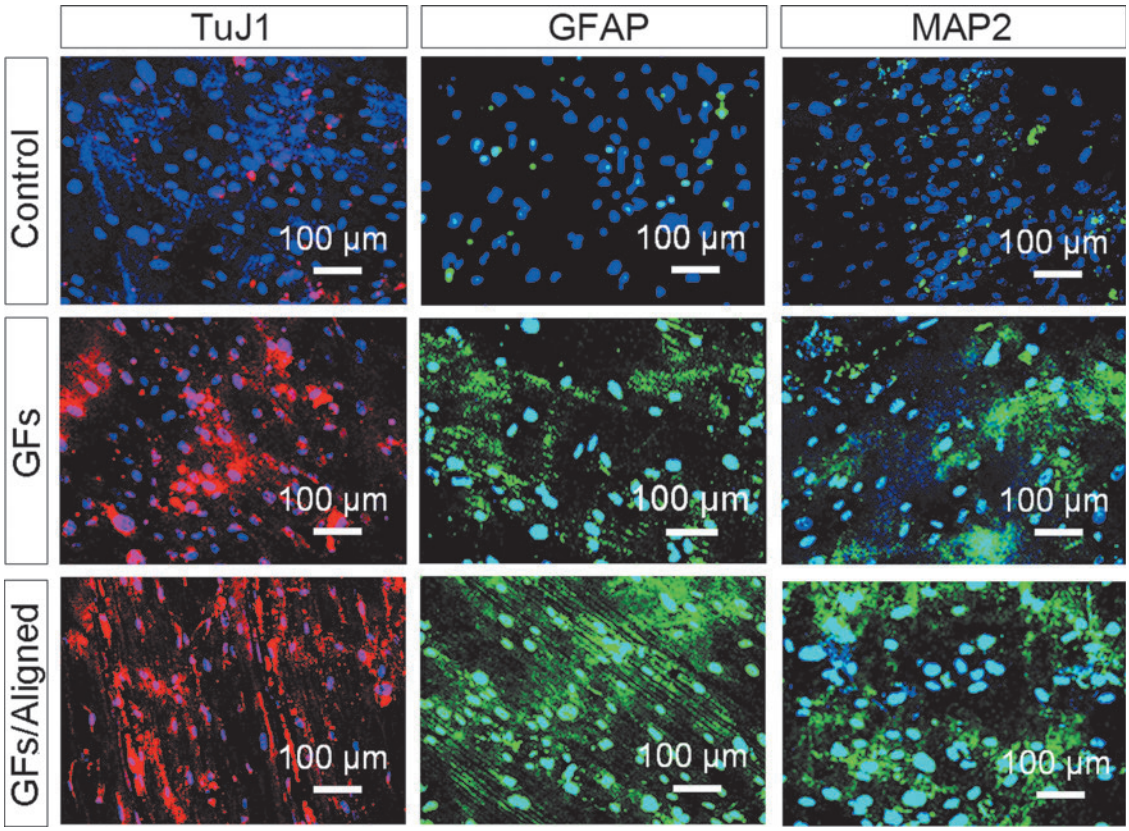

FIG. 7. hMSC-NSCs differentiation into neurons and astrocytes on different scaffolds for 2 weeks (DAPI, *blue*; TuJ1, *red*; GFAP/MAP2, *green*). Control, the noneated scaffolds without aligned patterns; GFs, pDA/GFs-coated scaffolds without aligned patterns; and GFs/Aligned, pDA/GFs-coated scaffolds with aligned patterns. DAPI, 4′,6-diamidino-2-phenylindole; GF, growth factor; GFAP, glial fibrillary acidic protein; hMSC-NSC, human mesenchymal stem cell-neural stem cell like cell; MAP2, microtubule-associated protein 2; pDA, polydopamine; TuJ1, class-III b-tubulin.

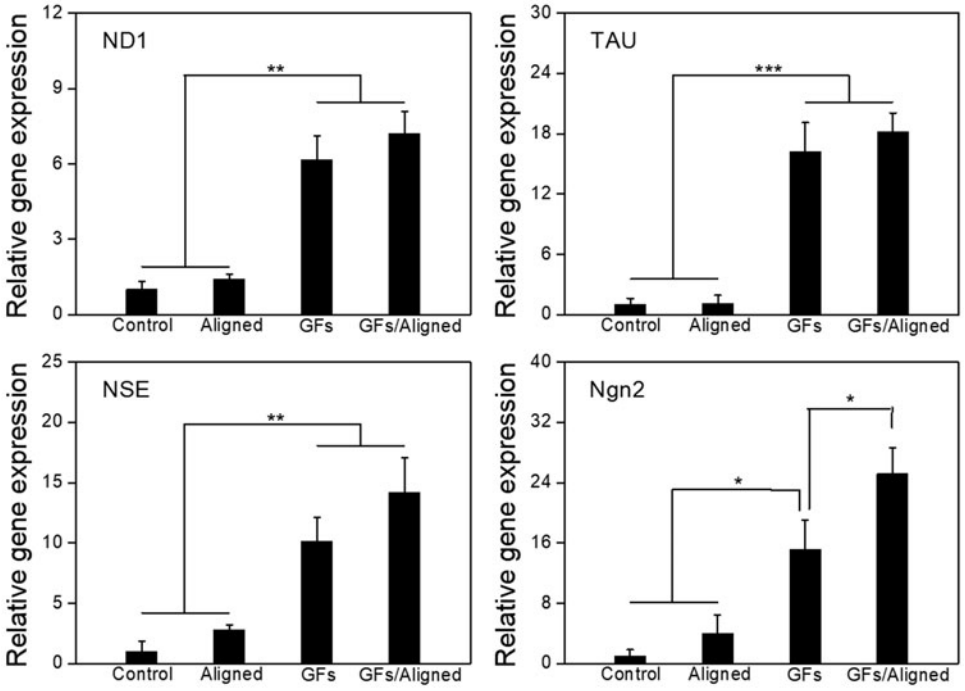

FIG. 8. Gene expression of neural differentiation of hMSCs for 4 weeks of differentiation induction culture. Control, the nontreated scaffolds without aligned patterns; Aligned, the nontreated scaffolds with aligned patterns; GFs, pDA/GFs-coated scaffolds without aligned patterns; and GFs/Aligned, pDA/GFs-coated scaffolds with aligned patterns. GF, growth factor; hMSCs, human mesenchymal stem cells; ND1, neurogenic differentiation 1; Ngn2, neurogenin 2; NSE, neuron-specific enolase; pDA, polydopamine; TAU, Tau proteins.

this process.[35–39] Immunostaining and PCR results demonstrated that the biological cue played a more crucial role in the neurogenic differentiation of hMSCs when compared with the topographic cues. Specific neuronal markers exhibited elevated expression on the aligned samples, indicating improved axon alignment of hMSCs during neuronal differentiation, in contrast to samples without microgrooves.

Due to a mismatch between the size and shape of our 4D scrolled conduits and the requirements of confocal microscopy, where the lens gap was significantly smaller than that of the 4D conduits, the complete images of the 4D scrolled conduits were not captured in our cell staining studies (Figs. 3, 5–7). While we do present cell images from specific local areas of the scaffolds, our findings effectively emphasize the combined impact of topographical features and GF immobilization. These elements provide instructive physical and biological cues that enhance the neural differentiation of hMSCs associated with axonal alignment. Thus, the aligned microgroove fabrication and mussel-inspired immobilization offer great potential for engineering nerve conduits to treat nerve injuries.

Conclusion

In this study, a novel nerve construct with aligned microgrooves has been fabricated using the PST printing technique. The combination of PL and SL printing resulted in well-defined micropatterns on the printed scaffolds, providing excellent advantages for guiding cell growth with orientation. A mussel-inspired pDA coating was then performed to immobilize GFs to improve the neural differentiation of resident hMSCs. The current study presents a novel strategy to develop multifunctional 4D nerve conduits, integrating topographic guidance and biological cues. This printed construct exhibits the potential for 4D shape-changing capacities, enabling dynamic self-entubulation and seamless integration for the development of smart nerve conduits.

Acknowledgments

The authors thank the George Washington University Center of Microscopy and Image Analysis for their assistance in image acquisition.

Authors' Contributions

H.C.: conceptualization (lead); investigation (lead); formal analysis (lead); methodology (lead); and writing—original draft (lead). W.Z.: conceptualization (equal); investigation (equal); and methodology (equal). S.M.: investigation (supporting) and methodology (supporting). K.S.: writing—review and editing (supporting). L.G.Z.: conceptualization (lead); supervision (lead), project administration (lead), and writing—review and editing (lead).

Disclosure Statement

No competing financial interests exist.

Funding Information

The authors thank the financial support from the NSF EBMS program grant 2110842.

References

1. Shen H, Fan C, You Z, et al. Advances in biomaterial-based spinal cord injury repair. Adv Funct Mater 2021;32(13); 2110628; doi: 10.1002/adfm.202110628
2. Huang L, Fu C, Xiong F, et al. Stem cell therapy for spinal cord injury. Cell Transplant 2021;30:963689721989266; doi: 10.1177/0963689721989266
3. Joung D, Lavoie NS, Guo SZ, et al. 3D printed neural regeneration devices. Adv Funct Mater 2020;30(1):1906237; doi: 10.1002/adfm.201906237
4. Lavorato A, Raimondo S, Boido M, et al. Mesenchymal stem cell treatment perspectives in peripheral nerve regeneration: Systematic review. Int J Mol Sci 2021;22(2): 572; doi: 10.3390/ijms22020572
5. Li M, Chen H, Zhu M. Mesenchymal stem cells for regenerative medicine in central nervous system. Front Neurosci 2022;16:1068114; doi: 10.3389/fnins.2022.1068114
6. Brown C, McKee C, Bakshi S, et al. Mesenchymal stem cells: Cell therapy and regeneration potential. J Tissue Eng Regen Med 2019;13(9):1738–1755; doi: 10.1002/term .2914
7. Zhang H, Guo J, Wang Y, et al. Natural polymer-derived bioscaffolds for peripheral nerve regeneration. Adv Funct Mater 2022;32(41):2203829; doi: 10.1002/adfm.202203829
8. Thibodeau A, Galbraith T, Fauvel CM, et al. Repair of peripheral nerve injuries using a prevascularized cell-based tissue-engineered nerve conduit. Biomaterials 2022;280: 121269; doi: 10.1016/j.biomaterials.2021.121269
9. Zhang S, Wang J, Zheng Z, et al. Porous nerve guidance conduits reinforced with braided composite structures of silk/magnesium filaments for peripheral nerve repair. Acta Biomater 2021;134:116–130; doi: 10.1016/j.actbio.2021.07.028
10. Tang Y, Xu Z, Tang J, et al. Architecture-engineered electrospinning cascade regulates spinal microenvironment to promote nerve regeneration. Adv Healthc Mater 2023; 12(12):e2202658; doi: 10.1002/adhm.202202658
11. Liu S, Xie YY, Wang LD, et al. A multi-channel collagen scaffold loaded with neural stem cells for the repair of spinal cord injury. Neural Regen Res 2021;16(11):2284–2292; doi: 10.4103/1673-5374.310698
12. Fan Z, Liao X, Tian Y, et al. A prevascularized nerve conduit based on a stem cell sheet effectively promotes the repair of transected spinal cord injury. Acta Biomater 2020;101:304–313; doi: 10.1016/j.actbio.2019.10.042
13. Sun X, Bai Y, Zhai H, et al. Devising micro/nano-architectures in multi-channel nerve conduits towards a pro-regenerative matrix for the repair of spinal cord injury. Acta Biomater 2019;86:194–206; doi: 10.1016/j.actbio .2018.12.032
14. Petcu EB, Midha R, McColl E, et al. 3D printing strategies for peripheral nerve regeneration. Biofabrication 2018;10(3): 032001; doi: 10.1088/1758-5090/aaaf50
15. Zhu W, Tringale KR, Woller SA, et al. Rapid continuous 3D printing of customizable peripheral nerve guidance conduits. Mater Today (Kidlington) 2018;21(9):951–959; doi: 10.1016/j.mattod.2018.04.001
16. Tao J, Zhang J, Du T, et al. Rapid 3D printing of functional nanoparticle-enhanced conduits for effective nerve repair. Acta Biomater 2019;90:49–59; doi: 10.1016/j.actbio.2019 .03.047
17. Bedir T, Ulag S, Ustundag CB, et al. 3D bioprinting applications in neural tissue engineering for spinal cord injury repair. Mater Sci Eng C Mater Biol Appl 2020;110:110741; doi: 10.1016/j.msec.2020.110741

Downloaded by UNIVERSITY OF SOUTHERN CALIFORNIA PACKAGE from www.liebertpub.com at 08/21/25. For personal use only.

Downloaded by UNIVERSITY OF SOUTHERN CALIFORNIA PACKAGE from www.liebertpub.com at 08/21/25. For personal use only.

18. Miao S, Castro N, Nowicki M, et al. 4D printing of polymeric materials for tissue and organ regeneration. Mater Today (Kidlington) 2017;20(10):577–591; doi: 10.1016/j.mattod.2017.06.005
19. Esworthy TJ, Miao S, Lee SJ, et al. Advanced 4D bioprinting technologies for brain tissue modeling and study. Int J Smart Nano Mat 2019;10(3):177–204; doi: 10.1080/19475411.2019.1631899
20. Hann SY, Cui HT, Nowicki M, et al. 4D printing soft robotics for biomedical applications. Addit Manuf 2020;36:101567; doi: 10.1016/j.addma.2020.101567
21. Agarwal T, Hann SY, Chiesa I, et al. 4D printing in biomedical applications: Emerging trends and technologies. J Mater Chem B 2021;9(37):7608–7632; doi: 10.1039/d1tb01335a
22. Wang Y, Cui H, Esworthy T, et al. Emerging 4D printing strategies for next-generation tissue regeneration and medical devices. Adv Mater 2022;34(20):e2109198; doi: 10.1002/adma.202109198
23. Miao S, Cui H, Nowicki M, et al. Stereolithographic 4D bioprinting of multiresponsive architectures for neural engineering. Adv Biosyst 2018;2(9):1800101; doi: 10.1002/adbi.201800101
24. Cui H, Miao S, Esworthy T, et al. A novel near-infrared light responsive 4D printed nanoarchitecture with dynamically and remotely controllable transformation. Nano Res 2019;12(6):1381–1388; doi: 10.1007/s12274-019-2340-9
25. Miao S, Cui H, Nowicki M, et al. Photolithographic-stereolithographic-tandem fabrication of 4D smart scaffolds for improved stem cell cardiomyogenic differentiation. Biofabrication 2018;10(3):035007; doi: 10.1088/1758-5090/aabe0b
26. Hann SY, Cui H, Esworthy T, et al. 4D thermo-responsive smart hiPSC-CM cardiac construct for myocardial cell therapy. Int J Nanomed 2023;18:1809–1821; doi: 10.2147/ijn.S402855
27. Cui H, Liu C, Esworthy T, et al. 4D physiologically adaptable cardiac patch: A 4-month in vivo study for the treatment of myocardial infarction. Sci Adv 2020;6(26):eabb5067; doi: 10.1126/sciadv.abb5067
28. Wang Y, Cui H, Wang Y, et al. 4D printed cardiac construct with aligned myofibers and adjustable curvature for myocardial regeneration. ACS Appl Mater Inter 2021;13(11):12746–12758; doi: 10.1021/acsami.0c17610
29. Miao S, Cui H, Esworthy T, et al. 4D self-morphing culture substrate for modulating cell differentiation. Adv Sci (Weinh) 2020;7(6):1902403; doi: 10.1002/advs.201902403
30. Joshi A, Choudhury S, Baghel VS, et al. 4D printed programmable shape-morphing hydrogels as intraoperative self-folding nerve conduits for sutureless neurorrhaphy. Adv Healthc Mater 2023:e2300701; doi: 10.1002/adhm.202300701
31. Lin Y, Yu J, Zhang Y, et al. 4D printed tri-segment nerve conduit using zein gel as the ink for repair of rat sciatic nerve large defect. Biomater Adv 2023;151:213473; doi: 10.1016/j.bioadv.2023.213473
32. Yang K, Lee JS, Kim J, et al. Polydopamine-mediated surface modification of scaffold materials for human neural stem cell engineering. Biomaterials 2012;33(29):6952–6964; doi: 10.1016/j.biomaterials.2012.06.067
33. Sun X, Cheng L, Zhao J, et al. bFGF-grafted electrospun fibrous scaffolds via poly(dopamine) for skin wound healing. J Mater Chem B 2014;2(23):3636–3645; doi: 10.1039/c3tb21814g
34. Cui H, Zhu W, Nowicki M, et al. Hierarchical fabrication of engineered vascularized bone biphasic constructs via dual 3D bioprinting: Integrating regional bioactive factors into architectural design. Adv Healthc Mater 2016;5(17):2174–2181; doi: 10.1002/adhm.201600505
35. Fu L, Zhu L, Huang Y, et al. Derivation of neural stem cells from mesenchymal stemcells: Evidence for a bipotential stem cell population. Stem Cells Dev 2008;17(6):1109–1121; doi: 10.1089/scd.2008.0068
36. Hermann A, Gastl R, Liebau S, et al. Efficient generation of neural stem cell-like cells from adult human bone marrow stromal cells. J Cell Sci 2004;117(Pt 19):4411–4422; doi: 10.1242/jcs.01307
37. Guan M, Xu Y, Wang W, et al. Differentiation into neurons of rat bone marrow-derived mesenchymal stem cells. Eur Cytokine Netw 2014;25(3):58–63; doi: 10.1684/ecn.2014.0357
38. Rafieemehr H, Kheirandish M, Soleimani M. Neural differentiation of human umbilical cord blood-derived mesenchymal stem cells. Avicenna J Med Biochem 2016 (in press); doi: 10.17795/ajmb-29066
39. Ahmedy E, Kandel S, Gabr H, et al. Neurogenic differentiation of bone marrow-derived mesenchymal stem cells using neural induction medium: A morphological and histochemical study. Am J Biosci Bioeng 2015;3(4):43–50; doi: 10.11648/j.bio.s.2015030401.17
40. Miao S, Zhu W, Castro NJ, et al. 4D printing smart biomedical scaffolds with novel soybean oil epoxidized acrylate. Sci Rep 2016;6:27226; doi: 10.1038/srep27226
41. Duenas F, Becerra V, Cortes Y, et al. Hepatogenic and neurogenic differentiation of bone marrow mesenchymal stem cells from abattoir-derived bovine fetuses. BMC Vet Res 2014;10:154; doi: 10.1186/1746-6148-10-154
42. Prabhakaran MP, Venugopal JR, Ramakrishna S. Mesenchymal stem cell differentiation to neuronal cells on electrospun nanofibrous substrates for nerve tissue engineering. Biomaterials 2009;30(28):4996–5003; doi: 10.1016/j.biomaterials.2009.05.057
43. Masters KS. Covalent growth factor immobilization strategies for tissue repair and regeneration. Macromol Biosci 2011;11(9):1149–1163; doi: 10.1002/mabi.201000505
44. Cui H, Zhu W, Huang Y, et al. In vitro and in vivo evaluation of 3D bioprinted small-diameter vasculature with smooth muscle and endothelium. Biofabrication 2019;12(1):015004; doi: 10.1088/1758-5090/ab402c

Address correspondence to:
Lijie Grace Zhang, PhD
Department of Mechanical and Aerospace Engineering
The George Washington University
Science and Engineering Hall 3590, 800 22nd Street NW
Washington, DC 20052
USA

E-mail: lgzhang@email.gwu.edu

Received: August 1, 2023
Accepted: October 10, 2023
Online Publication Date: November 15, 2023